ACS Catalysis

Research Article

pubs.acs.org/acscatalysis

Controlled Synthesis of Ultrafine Surfactant-Free NiPt Nanocatalysts toward Efficient and Complete Hydrogen Generation from Hydrazine Borane at Room Temperature

Qi-Long Zhu,[†] Di-Chang Zhong,[†] Umit B. Demirci,[‡] and Qiang Xu*[,†]

[†]National Institute of Advanced Industrial Science and Technology (AIST), 1-8-31 Midorigaoka, Ikeda, Osaka 563-8577, Japan

[‡]IEM (Institut Europeen des Membranes), UMR 5635 (CNRS-ENSCM-UM2), Universite Montpellier 2, Place E. Bataillon, F-34095, Montpellier, France

Supporting Information

ABSTRACT: A sodium-hydroxide-assisted reduction approach has been developed to control the synthesis of ultrafine surfactant-free bimetallic NiPt nanoparticles (NPs) supported on nanoporous carbon, Maxsorb MSC-30. For the first time, this catalyst exerts exceedingly high catalytic activity for 100% selective conversion of hydrazine borane (HB) to hydrogen at room temperature. This remarkably facile and effective reduction approach provides a powerful entry into ultrafine alloy NPs to make full use of noble metals and achieve enhanced performance, where the compositions of the alloy can be widely adjusted and tailored. Moreover, the catalytic results open up new avenues in the effective application of HB as a promising hydrogen storage material.

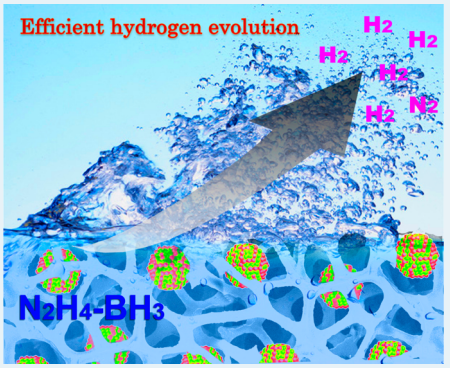

KEYWORDS: *hydrazine borane, hydrogen evolution, ultrafine nanoparticles, bimetallic, heterogeneous catalysis*

1. INTRODUCTION

Ultrafine metal nanoparticles (NPs) with extremely narrow size range have attracted particular interest due to their increased surface area and the number of edge and corner atoms, which greatly improve the catalytic properties.[1] However, as the surface energy increases with decreasing particle size, the syntheses of ultrafine nanoparticles remain a challenge in terms of particle size and distribution control, and catalyst stability under various operating conditions. In order to get well-dispersed metallic particles and protect them from agglomeration, organic surfactants have been widely used.[2] For instance, it has been reported that ultrafine and uniform alloy nanoparticles can be achieved by using dendrimers and oleylamines as stabilizing agents in the syntheses.[2a,e,f] Nevertheless, the exposed surface of nanocatalysts is often contaminated by the chemical interactions between the surfactant molecules and the catalyst surface in the process of preparation and therefore decreases the catalytic activities. For catalytic applications, general and facile methods that can easily control the nucleation and growth of the uncapped metal NPs with high uniformity, especially non-noble metal-based NPs, are highly desirable.

On the other hand, despite decades of extensive efforts, the search for effective on-board hydrogen storage materials with the combination of high gravimetric/volumetric hydrogen density and adequate kinetics remains one of the most challenging barriers on the path to a "hydrogen economy" society.[3] Since the early 2000s, boron-based chemical hydrogen storage materials, represented by the sodium borohydride ($NaBH_4$) and ammonia borane (NH_3BH_3), have been extensively studied owing to the lightness of boron.[4] Hydrolyses of $NaBH_4$ and NH_3BH_3 have attracted considerable attention because of their significant hydrogen contents (10.8 and 19.6 wt % H, respectively). Yet their technological implementation suffers from low effective material-based gravimetric hydrogen storage capacities (GHSC, 7.3 wt % in $NaBH_4$−$4H_2O$, eq 1 and 5.9 wt % in NH_3BH_3−$4H_2O$, eq 2) for consideration in vehicle applications. Recently, hydrous hydrazine ($N_2H_4{\cdot}H_2O$), a liquid at room temperature having high hydrogen capacity (8.0 wt %), has been identified as a potential liquid-phase chemical hydrogen storage material, whereas the safety issues due to its volatility and toxicity need to be solved for practical use.[5]

$$NaBH_4 + 4H_2O \longrightarrow NaB(OH)_4 + 4H_2 \quad (1)$$

$$NH_3BH_3 + 4H_2O \longrightarrow NH_4B(OH)_4 + 3H_2 \quad (2)$$

$$N_2H_4BH_3 + 3H_2O \longrightarrow N_2H_4 + B(OH)_3 + 3H_2 \quad (3a)$$

$$N_2H_4 \longrightarrow N_2 + 2H_2$$

$$3N_2H_4 \longrightarrow 4NH_3 + N_2 \quad (3b)$$

Received: August 22, 2014
Revised: October 15, 2014
Published: October 21, 2014

   dx.doi.org/10.1021/cs501329c | ACS Catal. 2014, 4, 4261−4268

Hydrazine borane (HB, $N_2H_4BH_3$), a stable and safe solid at room temperature having hydrogen content as high as 15.4 wt %, has high potential for use as a high-performance hydrogen storage material.[6−8] It can be prepared by mixing sodium borohydride and hydrazine hemisulfate at room temperature and obtained at high purity (i.e., 99%) in our conditions.[6c] A strategy combining hydrolysis of the group BH_3 and selective decomposition of the moiety N_2H_4 to N_2 and H_2 (eq 3a) might be a promising approach for complete dehydrogenation of HB.[7] This corresponds to a theoretical GHSC of 10.0 wt % for the system $HB−3H_2O$, which is much higher than those of $NaBH_4−4H_2O$ and $NH_3BH_3−4H_2O$. With suitable catalysts, it is expected to readily hydrolyze the group BH_3 in an aqueous solution at room temperature, producing hydrazine N_2H_4, in comparison with the formation of ammonia NH_3 in the hydrolysis of ammonia borane. Furthermore, the in situ formed hydrazine can be selectively decomposed to N_2 and H_2 in the presence of appropriate catalysts, which makes HB more attractive than AB. However, to maximize the efficacy of HB as a hydrogen storage material, one must avoid the undesired reaction pathway given by eq 3b. Recently, a few surfactant-stabilized nanocatalysts have been synthesized to catalyze the dehydrogenation of HB, but they display incomplete hydrogen selectivity and slow kinetics even at elevated temperatures (50 °C).[7a,8] Therefore, it is critical to develop new catalysts that exhibit high catalytic performance to both hydrolysis of the group BH_3 and selective decomposition of the moiety N_2H_4 under moderate conditions for establishment of the hydrogen storage system based on HB.

Owing to its inherent advantages such as accessible porosity, large surface area, high chemical and thermal stability, nanoporous carbon, Maxsorb MSC-30 (pore size, 2.1 nm; BET surface area, ∼3000 $m^2\ g^{-1}$) has capabilities that make it superior to organic surfactants as support for high-performance nanocatalysts.[9] Moreover, the anchoring of nanocatalysts on MSC-30 could be capable of facilitating the electron transfer and mass transport kinetics during the catalytic reaction process.[9b] Herein, encouraged by the catalytic performance of the NiPt system having shown hydrogen selectivity up to 100% in the dehydrogenation of hydrous N_2H_4,[5e,10] we synthesized MSC-30 supported NiPt nanocatalyst by using a facile one-pot sodium-hydroxide-assisted reduction approach in the presence of sodium hydroxide, which played a key role to achieve ultrafine NiPt alloy NPs via generating intermediate nickel hydroxide gel during the reduction process (Figure 1). Surprisingly, the resultant surfactant-free nanocatalyst is the first one exerting 100% hydrogen selectivity and exceedingly high activity toward complete conversion of hydrazine borane to hydrogen via hydrolysis of BH_3 and decomposition of N_2H_4 at room temperature.

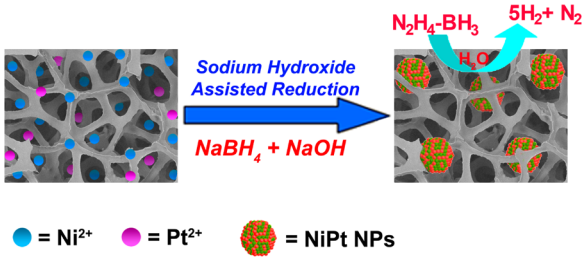

Figure 1. Schematic representation for the preparation of NiPt/MSC-30 nanocatalyst via a sodium-hydroxide-assisted reduction approach and gas (H_2 + N_2) evolution from the dehydrogenation of HB.

2. EXPERIMENTAL SECTION

2.1. Chemicals and Materials. Hydrazine borane (HB) was synthesized according to the reported literature.[7a] The other chemicals were purchased and used without further purification. Nickel chloride hexahydrate ($NiCl_2·6H_2O$, Wako Pure Chemical Industries, Ltd., 99%), potassium tetrachloroplatinate (K_2PtCl_4, Wako Pure Chemical Industries, Ltd., >98%), sodium borohydride ($NaBH_4$, Sigma-Aldrich, 99%), sodium hydroxide (NaOH, Chameleon Reagent, >98%), Maxsorb MSC-30 (Nanoporous Carbon, Kansai Coke and Chemicals Co. Ltd.), and cetyltrimethylammonium bromide (CTAB, Sigma-Aldrich, 95%) were used as received. Deionized water with a specific resistance of 18.2 MΩ·cm was obtained by reverse osmosis followed by ion-exchange and filtration (RFD 250NB, Toyo Seisakusho Kaisha, Ltd., Japan).

2.2. Syntheses of Catalysts. The NiPt nanoparticles supported by MSC-30 were synthesized by a facile sodium-hydroxide-assisted reduction method. Typically, 100 mg of MSC-30 carbon powder in a two-necked round-bottomed flask was ultrasonically dispersed in 2.5 mL of water and subsequently mixed with an aqueous solution of K_2PtCl_4 and/or $NiCl_2$ with desired concentrations. The resultant aqueous suspension was further homogenized under sonication for 30 min. Then, 12 mg of $NaBH_4$ dissolved in 1.0 mL of 3.0 M NaOH solution was added into the above obtained solution with vigorous shaking, resulting in the generation of catalyst as a dark suspension. The molar ratios of $Pt^{2+}/(Pt^{2+} + Ni^{2+})$ were changed with several values (0, 0.05, 0.15, 0.30, 0.40, 0.50. 0.70, 1.00), while the molar contents of $(Pt^{2+} + Ni^{2+})$ added to 100 mg of MSC-30 matrix were kept at 0.10 mmol. The catalysts with different Pt/Ni molar ratios were denoted as $Ni_{1-x}Pt_x$/MSC-30.

For comparison, another catalyst with Ni/Pt molar ratio of 6:4 was prepared using the same synthetic procedure but in the absence of NaOH, which was denoted as $Ni_{0.6}Pt_{0.4}$/MSC-30_N.

2.3. Instrumentation. Laboratory powder X-ray diffraction patterns were collected for synthesized catalysts on a Mac Science MXP3 V diffractometer with Ni-filtered Cu Kα radiation (λ = 0.15406 nm; 40 kV, 20 mA). The surface area measurements were performed with N_2 adsorption/desorption isotherms at liquid nitrogen temperature (77 K) after dehydration under vacuum at 120 °C for 12 h using automatic volumetric adsorption equipment (Belsorp-max). X-ray photoelectron spectroscopic (XPS) measurements were conducted on a Shimadzu ESCA-3400 X-ray photoelectron spectrometer using an Mg Kα source (10 kV, 10 mA). The argon sputtering experiments were carried out under the conditions of background vacuum of 3.2×10^{-6} Pa and sputtering acceleration voltage of 2 kV and sputtering current of 10 mA. Charging of the catalyst samples was corrected by setting the binding energy of the adventitious carbon (C 1s) at 284.6 eV. The TEM and HAADF-STEM images and the EDX spectra were recorded on transmission electron microscope (TEM, TECNAI G^2 F20) with operating voltage at 200 kV equipped with energy-dispersive X-ray (EDX) detector. Mass analysis of the generated gases was performed using a Balzers Prisma QMS 200 mass spectrometer. UV−vis absorption spectra were recorded on a Shimadzu UV-2550 spectrophotometer and corrected by deionized water as background absorption.

dx.doi.org/10.1021/cs501329c | ACS Catal. 2014, 4, 4261−4268

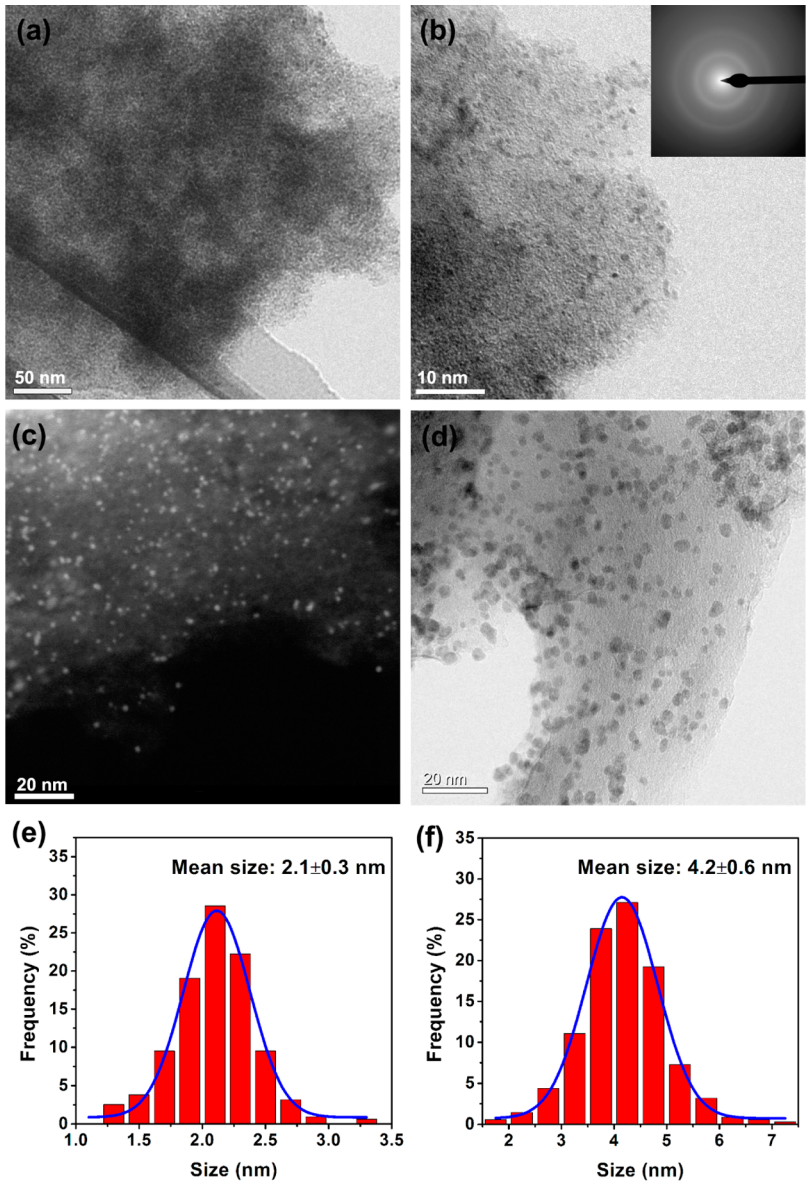

Figure 2. (a,b) TEM and (c) HAADF-STEM images of $Ni_{0.6}Pt_{0.4}$/MSC-30, (d) TEM image of $Ni_{0.6}Pt_{0.4}$/MSC-30_N, and size distribution histograms of (e) $Ni_{0.6}Pt_{0.4}$/MSC-30 and (f) $Ni_{0.6}Pt_{0.4}$/MSC-30_N.

2.4. Catalysis. The reaction apparatus for measuring the H_2/N_2 evolution from HB is the same as previously reported.[7b] Typically, the two-necked round-bottomed flask (30 mL) with the as-synthesized catalyst was placed in a water bath at 30 °C under ambient atmosphere. A gas buret filled with water was connected to the reaction flask to measure the volume of released gas (lab temperature kept constant at 25 °C during measurements). The reaction started under shaking when 1.0 mL of aqueous solution containing 1.0 mmol HB was injected into the mixture using a syringe. The volume of the evolved hydrogen gas was monitored by recording the displacement of water in the gas buret. The reaction was completed when there was no more gas generation. The molar ratios of (Ni + Pt)/HB were theoretically fixed at 0.10 for all the catalytic reactions.

Durability of the Catalysts. For testing the durability of the catalyst $Ni_{0.6}Pt_{0.4}$/MSC-30, an aliquot of HB in 1.0 mL of 1.0 M NaOH solution was subsequently added into the reaction flask after the completion of the last run. This cycling test for the catalytic dehydrogenation of HB was carried out for five runs at 30 °C.

Stability of the Catalysts. After the reaction, the catalyst $Ni_{0.6}Pt_{0.4}$/MSC-30 was separated from the reaction solution by centrifugation, which was washed three times with water, and then dried under vacuum at room temperature for the PXRD and TEM analyses.

2.5. Calculation Methods for Kinetics. The metal dispersion (D_M) value is defined as the ratio of the number of surface atoms to the total number of atoms. For the supported metal catalyst, the metal dispersion was calculated on the basis of the average particle diameter by using the equation:[11]

$$D_M = \frac{6n_sM}{\rho N d_P}$$

Where n_s is the number of metal atoms on the surface per unit area (1.25×10^{19} m^{-2} for Pt, and 1.54×10^{19} m^{-2} for Ni), M is the molecular weight (195.08 g mol^{-1} for Pt, and 58.69 g mol^{-1}

dx.doi.org/10.1021/cs501329c | ACS Catal. 2014, 4, 4261−4268

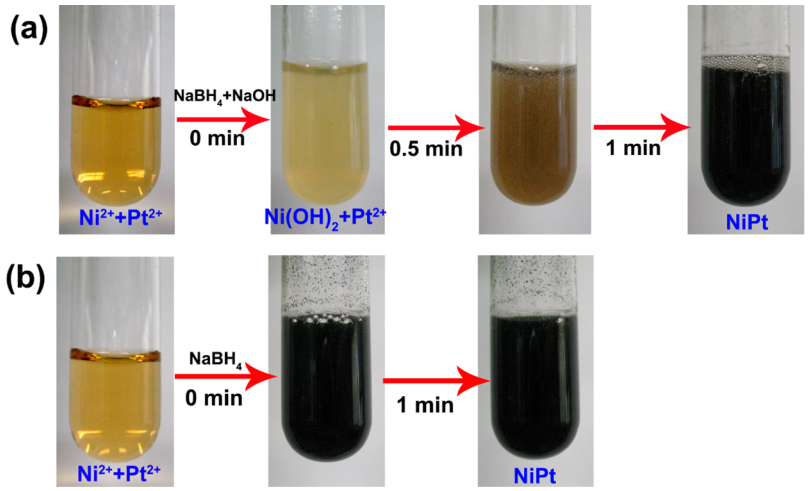

Figure 3. Color changes of the aqueous solution of Ni^{2+} and Pt^{2+} during the reduction processes in the (a) presence and (b) absence of NaOH.

for Ni), ρ is the density (21.35 g cm^{-3} for Pt, and 8.91 g cm^{-3} for Ni), N is 6.023×10^{23} mol^{-1}, and d_p is the average particle diameter measured by TEM. The average values of these parameters were used to calculate the metal dispersion of NiPt considering the molar ratio of Ni to Pt in the catalysts.

The kinetics of hydrogen generation in this work was evaluated by using site-time- yield (STY) value, which is defined as the number of molecules of a specified product made per catalytic site per unit time.[12] STY was calculated from the equation:

$$\mathrm{STY} = \frac{5P_{\mathrm{atm}}V_{\mathrm{gas}}/RT}{6D_{\mathrm{M}}n_{\mathrm{metal}}t}$$

where P_{atm} is the atmospheric pressure (101 325 Pa), V_{gas} is the final volume of generated H_2/N_2 gas, R is the universal gas constant (8.3145 m^3 Pa mol^{-1} K^{-1}), T is the room temperature (298 K), D_M is the metal dispersion, n_{metal} is the total mole number of NiPt atoms in catalyst, and t is the completion time of the reaction.

3. RESULTS AND DISCUSSION

The surfactant-free NiPt alloy NPs supported on MSC-30 were synthesized by coreduction of nickel(II) chloride and potassium hexachloroplatinum (II) in the presence of MSC-30 using an alkaline solution of sodium borohydride as a reductant. The resulting $Ni_{1-x}Pt_x$/MSC-30 was used for catalytically releasing H_2 from HB. Because the preparation of NiPt catalysts was carried out in a reductive condition without exposure to air, which then were used for the dehydrogenation of HB immediately, the oxidation of nickel has been mostly avoided. The catalyst with the Ni/Pt atomic ratio of 6:4 exhibited the highest activity (vide infra), and therefore, $Ni_{0.6}Pt_{0.4}$/MSC-30 was chosen as the model catalyst to explore the effect of sodium hydroxide on the distribution of the nanoparticles. For comparison, $Ni_{0.6}Pt_{0.4}$/MSC-30_N was also prepared in the absence of NaOH.

The microstructures of $Ni_{0.6}Pt_{0.4}$/MSC-30 and $Ni_{0.6}Pt_{0.4}$/MSC-30_N catalysts were investigated with a full characterization. The transmission electron microscopy (TEM) and high-angle annular dark-field scanning TEM (HAADF-STEM) images of $Ni_{0.6}Pt_{0.4}$/MSC-30 show that the NiPt NPs are highly dispersed into the framework of MSC-30 with an average particle size of 2.1 ± 0.3 nm based on TEM observations (Figure 2a–c and 2e). The corresponding selected area energy dispersion (SAED) pattern indicates the crystalline nature of the Pt NPs (inset in Figure 2b). When the NiPt NPs were loaded without NaOH, a larger average particle size of 4.2 ± 0.6 nm was observed with some severely aggregated particles (Figures 2d,f and S5). However, the X-ray diffraction (XRD) and X-ray photoelectron spectroscopy (XPS) analyses show that the two catalysts possess similar crystallinity and electronic structures (Figures S2–S3). The XRD patterns of both catalysts display primarily the characteristics of the face-centered cubic (fcc) Pt with slight shift to higher angles with respect to those of Pt/MSC-30, suggesting a lattice contraction and alloy formation between Pt and Ni because platinum is known to alloy well with nickel.[13] The presence of NiPt NPs was also verified by N_2 sorption. In comparison to metal-free MSC-30, appreciable decreases in the amount of N_2 adsorption for both catalysts were observed (Figure S1). In addition, the larger decrease of surface area for $Ni_{0.6}Pt_{0.4}$/MSC-30 is attributed to the occupation of the dispersed size-matched NiPt NPs in the mesopores (~2.2 nm) of MSC-30. The particles in the confined cavities of MSC-30 can be protected from aggregation and thus may provide higher catalytic stability and durability. However, due to the particle size larger than the pore size of the carbon support, NiPt NPs in $Ni_{0.6}Pt_{0.4}$/MSC-30_N should be almost located on the surface of the MSC-30 framework.

Therefore, NaOH serves as an efficient dispersing agent to control the size distribution during the growth of NiPt NPs. For further making clear the role of NaOH in the catalyst formation, we tried to gather insight into the changes of the metal precursors during the reduction process by monitoring the color changes. To eliminate the color disturbance of carbon, only an aqueous solution of the metal precursors was used. As shown in Figure 3, contrary to the fast reduction of Ni^{2+} and Pt^{2+} by $NaBH_4$, upon the introduction of the NaOH and $NaBH_4$ mixture to the aqueous Ni^{2+} and Pt^{2+} solution, the fast generation of $Ni(OH)_2$ gel occurred preferentially prior to the reduction. The hydrated Pt^{2+} ions would be simultaneously converted into the chlorohydroxypallatium(II) species upon the addition of NaOH, for example, $PtCl(OH)(H_2O)_2$ or $PtCl_2(OH)(H_2O)^-$, which could be stable for a long time (1–2 days).[14] Subsequently, the hydroxide intermediate acted as precursor and capping agent in the successive reduction to prevent the resulting NiPt NPs from aggregation, leading to the

dx.doi.org/10.1021/cs501329c | ACS Catal. 2014, 4, 4261–4268

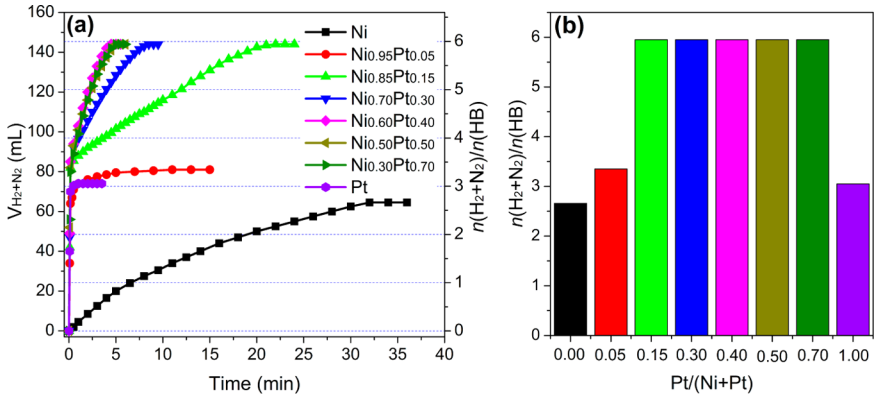

Figure 4. (a) Volume of the generated gas ($H_2 + N_2$) versus time and (b) Pt-content dependence of $n(H_2 + N_2)/n(HB)$ for the dehydrogenation of HB over NiPt/MSC-30 with different Ni/Pt molar ratios prepared with NaOH (n_{metal}/n_{HB} = 0.1, 30 °C).

Table 1. Catalytic Activities for Dehydrogenation of Hydrazine Borane Catalyzed by Different Heterogeneous Catalysts[a]

catalyst	n(metal)/n(HB)	temp (°C)	$n(H_2 + N_2)/n$(HB)	H_2 generation rate (L_{H2} h^{-1} g_{metal}^{-1})	ref
$Ni_{0.6}Pt_{0.4}$/MSC-30	**0.1**	**30**	**5.95 ± 0.05**	**142**	**this work**
Rh_4Ni/CTAB	0.1	50	5.80 ± 0.20	24	7b
$Ni_{0.89}Pt_{0.11}$/CTAB	0.14	50	5.79 ± 0.05	7	7a
$Ni_{0.77}Ru_{0.23}$/CTAB	0.15	50	4 ± 0.05	very low	8a
$Ni_{0.89}Rh_{0.11}$/CTAB	0.16	50	5.1 ± 0.05	very low	8a
$Ni_{0.89}Ir_{0.11}$/CTAB	0.14	50	4.9 ± 0.05	very low	8a
$RhCl_3$ precatalyst	0.013	50	4.1	very low	8b
$RuCl_3$ precatalyst	0.013	50	3.3	very low	8b
$IrCl_3$ precatalyst	0.013	50	3.3	very low	8b

[a]The catalysts that can only release the hydrogen from the BH_3 group of HB are not included.

formation of ultrafine NPs. In the process of reduction, the first-seeded Pt atoms are catalytically active for hydrogen generation by hydrolysis of sodium borohydride; this is accompanied by the generation of the intermediate Pt−H species, which act as a reducing agent for the reduction of nickel hydroxide and thus lead to the formation of NiPt NPs, as evidenced by the XPS measurement (Figure S3a).[15] The reduction of Ni^{2+} and Pt^{2+} also has been followed by UV−vis spectroscopy. From the UV−vis spectra of the monitoring for the reduction process of NiPt NPs at different reaction times (Figure S14), it can be found that the intensity of the strong absorption of Pt^{2+} species was maintained even after the addition of the alkaline solution of sodium borohydride for 20 s. The phenomena further suggest that the reduction of Ni^{2+} and Pt^{2+} took place after generating the nickel hydroxide intermediate. Besides the formation of $Ni(OH)_2$ species, the stabilization of $NaBH_4$ in basic solution might also make the nucleation process more controllable. In contrast, the tentative reduction of aqueous Ni^{2+} by $NaBH_4$ in alkaline conditions only resulted in the light-green precipitation of $Ni(OH)_2$; in other words, Ni^{2+} as $Ni(OH)_2$ cannot be reduced by sodium borohydride, as evidenced by the XRD, XPS and TEM measurement (Figures S2, S3e, S6c,d, and S13). In addition, the Ni/Pt molar ratio in the catalysts was also found to be important for the particle size distribution. The TEM measurement demonstrated that the NiPt NPs in catalysts obtained with the Ni/Pt molar ratios more than 1:1 are highly dispersed (Figure S7a−d). Although the Ni/Pt molar ratio was decreased to less than 1:1, a larger NiPt particle size and broader size distribution were observed (Figure S7e, f), which may be due to the fact that the amount of $Ni(OH)_2$ intermediate first generated was not sufficient to efficiently disperse the Pt species and prevent the aggregation of the final metal NPs.

The catalytic activity of $Ni_{1-x}Pt_x$/MSC-30 prepared in the presence of NaOH for HB dehydrogenation has been investigated at room temperature with a constant molar ratio of catalyst/HB = 1:10. It has been found that the catalytic activity and selectivity to hydrogen strongly depend on the Ni/Pt ratio (Figure 4). The dehydrogenation of HB was initiated by the introduction of aqueous HB solution into the reaction flask with vigorous shaking at room temperature. The released gas was measured volumetrically, and its composition was analyzed by mass spectrometry. Both monometallic Ni and Pt nanocatalysts showed activity for hydrogen release by hydrolysis of the BH_3 group in HB only, whereas the $Ni_{1-x}Pt_x$/MSC-30 nanocatalysts with platinum contents in the range of 15−70 mol % exhibited high catalytic activities and 100% hydrogen selectivity with 5.95 ± 0.05 equiv ($H_2 + N_2$) per HB released. This exceptional catalytic performance demonstrates that the resulting synergistic effect between Ni and Pt is required for the complete conversion of HB to H_2. A detailed analysis of the results in Figure 4 shows that the catalytic activity of $Ni_{1-x}Pt_x$/MSC-30 is first improved with the increasing content of Pt and reaches the maximum at 0.4. Then, when the Pt content further increases, the tendency reverses. These catalysts with 15−70 mol % Pt exhibit analogous time course profiles with a process composed of two distinct steps with different kinetics. The first step proceeds fast, where slightly more than 3.0 equiv H_2 evolves in less than 0.5 min, corresponding to the hydrolysis of the BH_3 group. The second step, the decomposition of the N_2H_4 moiety, is much slower, which determines the time that is needed by the entire dehydrogenation process of HB. It is observed that all the

dx.doi.org/10.1021/cs501329c | ACS Catal. 2014, 4, 4261−4268

catalysts prepared by our method show much better activity and selectivity compared to the previously reported analogous NiPt nanocatalysts stabilized by CTAB (Table 1).[7a]

The $Ni_{0.6}Pt_{0.4}$/MSC-30 catalyst was most active and efficiently and completely released gases in a stoichiometric amount (5.95 ± 0.05 equiv) from HB in 4.5 min (n_{metal}/n_{HB} = 0.1) at room temperature (Figure 4). The gases were identified by mass spectrometry to be hydrogen and nitrogen with a H_2/N_2 ratio of 5.0 (Figure S11), in agreement with the volumetric observations of 100% selectivity for hydrogen. The average rate of H_2 production was determined to be 142 L_{H2} h^{-1} g_{metal}^{-1}, corresponding to a theoretical power density of 192 W h^{-1} g_{metal}^{-1} for energy generation.[9b] Particularly noteworthy is that after calibration of the size of the nanocatalyst (i.e., ca. 2.1 nm for $Ni_{0.6}Pt_{0.4}$/MSC-30, corresponding to the metal dispersion (D_M) of approximately 50%), the site-time yield of H_2 was calculated to be 0.37 s^{-1} at 30 °C, which is much higher than those of the most active Rh_4Ni catalysts reported for this reaction even at high temperatures (Table 1).[7b] Meanwhile, $Ni_{0.6}Pt_{0.4}$/MSC-30 showed much higher H_2 selectivity and is cheaper compared to Rh_4Ni (it contains only 40% Pt compared to 80% Rh). It was found that there were some decreases in activity over five cycles (Figure S12), which may be due to the slight increase in the particle size of NiPt NPs during the catalytic process (Figures S15, S16). Nevertheless, $Ni_{0.6}Pt_{0.4}$/MSC-30_N can only release 3 equiv of H_2; even after adding the same amount of NaOH as an important catalyst promoter (vide infra), it still exhibited much lower catalytic activity than that of $Ni_{0.6}Pt_{0.4}$/MSC-30 (Figure S8). It has been known that the catalytic activity generally increases with the decrease in metal NPs size, as smaller particles possess higher surface areas available for reactants.[1c,9b] Reasonably, the decrease in the particle size of NiPt NPs on MSC-30 due to the presence of NaOH should be responsible for the exceedingly high activity of $Ni_{0.6}Pt_{0.4}$/MSC-30. It is also concluded that the alkaline additive is extremely important for the catalyst preparation to improvement of kinetics, which not only serves as an efficient dispersing agent to control the particle size during the formation of NiPt NPs in the present system but also plays a crucial role as a catalyst promoter to improve the catalytic performance.

It should be noted that a lower catalytic activity was observed over the $Ni_{0.6}Pt_{0.4}$/MSC-30 catalyst for the decomposition of $N_2H_4{\cdot}H_2O$ than that for the dehydrogenation of HB under the same condition (Figure 5). It took 6.5 min to completely decompose the same amount of $N_2H_4{\cdot}H_2O$ (1.0 mmol) as that resulted from the second step of the HB dehydrogenation reaction. According to a previous work, the $B(OH)_3$ formed in the first step has no influence on the decomposition of N_2H_4.[7b] Thus, the results reported here indicate that the dehydrogenation of HB is not simply divided into two steps in this catalytic reaction. A plausible explanation is that when the BH_3 group of HB is catalytically hydrolyzed by $Ni_{0.6}Pt_{0.4}$, concurrently, some of the resulting N_2H_4 moieties directly interact with metal NPs to generate N_2 and H_2, thus promoting the kinetic properties of HB dehydrogenation.

To determine the significant effect of the surfactant-free nature of NiPt NPs on the catalytic activity, surfactant cetyltrimethylammonium bromide (CTAB) supported $Ni_{0.6}Pt_{0.4}$ nanocatalyst ($Ni_{0.6}Pt_{0.4}$/CTAB) was prepared using our recently reported procedure, which gave NiPt NPs with an average size of ~3.5 nm.[16] Surprisingly, despite their similar particle size, the catalytic activity of the surfactant-protected

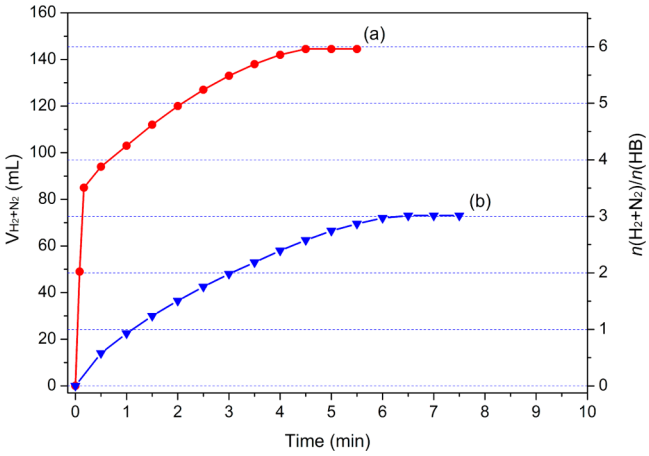

Figure 5. Volume of the generated gas (H_2 + N_2) versus time for the dehydrogenation of (a) HB and (b) $N_2H_4{\cdot}H_2O$ over $Ni_{0.6}Pt_{0.4}$/MSC-30 ($n_{metal}/n_{HB\ or\ N2H4\text{-}H2O}$ = 0.1, 30 °C).

NiPt NPs was much lower than that of surfactant-free ones for HB dehydrogenation (Figure S10). The observations further confirm that the absence of any protective surfactants, especially a hydrophobic surfactant shell around the metal NPs in an aqueous reaction medium, significantly benefits the access of reactants to the metal surface and therefore benefits the catalytic activity.

Besides the good dispersion and the surfactant-free character of the $Ni_{0.6}Pt_{0.4}$ NPs immobilized by MSC-30, the presence of NaOH plays an important role in promoting the catalytic performance. After washing away the NaOH present in the synthesis process of $Ni_{0.6}Pt_{0.4}$/MSC-30, the selectivity and activity of the catalyst decreased significantly with only 4.0 equiv of gases released even after 20 min (Figure S9). This indicates that NaOH has indeed a galvanizing impact on the selectivity and activity of the dehydrogenation of HB. Similarly, for $Ni_{0.6}Pt_{0.4}$/MSC-30_N catalyst without NaOH, only 3.0 equiv of gases was permitted to release, which originated only from hydrolysis of the BH_3 group, while the addition of NaOH could obviously improve the catalytic performance of $Ni_{0.6}Pt_{0.4}$/MSC-30_N, further confirming the promotion effect of NaOH (Figure S8). To determine the effect of the amount of NaOH on the catalytic performance, we have synthesized MSC-30 supported $Ni_{0.6}Pt_{0.4}$ NPs with various concentrations of NaOH (0−4 M). It has been found that the selectivity and activity of the catalysts for the dehydrogenation of HB increased with the concentration of NaOH until the value reached 3M, after which a further increase in the amount of NaOH showed little effect on the dehydrogenation of HB (Figure 6). As HB is very stable in the solution of MSC-30 and NaOH, NaOH only serves as a catalyst promoter for the decomposition of the N_2H_4 moiety in the second step of this reaction. The possible reason for the effects of the alkaline additive may be understood as follows: (a) the addition of NaOH could decrease the concentration of undesirable $N_2H_5^+$ ($N_2H_5^+ + OH^- \leftrightarrow N_2H_4 + H_2O$) and promote the rate-determining deprotonation step ($N_2H_4 \rightarrow N_2H_3^* + H^*$) along the decomposition process of N_2H_4 to N_2 and H_2; (b) the alkaline solution makes the catalyst surface highly basic, which helps inhibit the formation of basic NH_3 and therefore benefits the high H_2 selectivity.

dx.doi.org/10.1021/cs501329c | ACS Catal. 2014, 4, 4261−4268

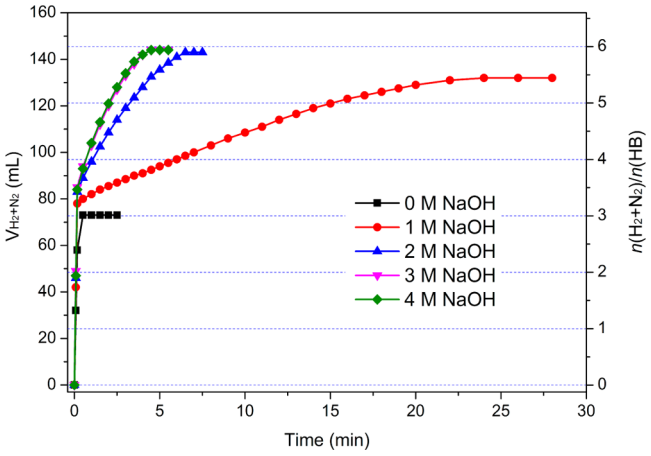

Figure 6. Volume of the generated gas (H_2 + N_2) versus time for the dehydrogenation of HB over $Ni_{0.6}Pt_{0.4}$/MSC-30 prepared with different concentrations of NaOH solution (1.0 mL) added (n_{metal}/n_{HB} = 0.1, 30 °C).

4. CONCLUSIONS

In summary, for the first time, a surfactant-free NiPt bimetallic nanocatalyst with good dispersion, prepared by using a sodium-hydroxide-assisted reduction approach in the presence of MSC-30, exhibits remarkable catalytic activity for efficient and complete dehydrogenation of hydrazine borane at room temperature, wherein NaOH not only serves as an efficient dispersing agent to control the particle size during the formation of NiPt NPs but also plays an important role as a catalyst promoter. The utilization of the sodium-hydroxide-assisted reduction approach to obtain ultrafine alloy nanoparticles opens up new avenues for designing highly efficient nanocatalysts. Meanwhile, the obtained catalyst is believed to give a tremendous boost to the practical application of hydrazine borane for chemical hydrogen storage with high material-based GHSC of 10.0%.

■ ASSOCIATED CONTENT

Supporting Information

The following files are available free of charge on the ACS Publications website at DOI: 10.1021/cs501329c.

PXRD, BET, XPS, TEM, EDX for catalysts; results of catalytic HB dehydrogenation; durability and stability results of catalysts (PDF).

■ AUTHOR INFORMATION

Corresponding Author

*E-mail: q.xu@aist.go.jp. Tel: +81-72-751-9562. Fax: +81-72-751-9629.

Notes

The authors declare no competing financial interest.

■ ACKNOWLEDGMENTS

The authors are thankful to the reviewers for valuable suggestions, Dr. Takeyuki Uchida for TEM measurements, and AIST and JSPS for financial support. Q.L.Z. thanks the JSPS for a postdoctoral fellowship.

■ REFERENCES

(1) (a) Chen, X.; Wu, G.; Chen, J.; Chen, X.; Xie, Z.; Wang, X. *J. Am. Chem. Soc.* **2011**, *133*, 3693−3695. (b) Kundu, P.; Nethravathi, C.; Deshpande, P. A.; Rajamathi, M.; Madras, G.; Ravishankar, N. *Chem. Mater.* **2011**, *23*, 2772−2780. (c) Zhu, Q.-L.; Li, J.; Xu, Q. *J. Am. Chem. Soc.* **2013**, *135*, 10210−10213. (d) Kim, B. H.; Hackett, M. J.; Park, J.; Hyeon, T. *Chem. Mater.* **2014**, *26*, 59−71. (e) Shang, L.; Bian, T.; Zhang, B.; Zhang, D.; Wu, L.-Z.; Tung, C.-H.; Yin, Y.; Zhang, T. *Angew. Chem., Int. Ed.* **2014**, *53*, 250−254.

(2) (a) Scott, R. W. J.; Wilson, O. M.; Oh, S.-K.; Kenik, E. A.; Crooks, R. M. *J. Am. Chem. Soc.* **2004**, *126*, 15583−15591. (b) Ye, H.; Crooks, R. M. *J. Am. Chem. Soc.* **2005**, *127*, 4930−4934. (c) Scott, R. W.; Wilson, O. M.; Crooks, R. M. *J. Phys. Chem. B* **2005**, *109*, 692−704. (d) Takahashi, M.; Imaoka, T.; Hongo, Y.; Yamamoto, K. *Angew. Chem., Int. Ed.* **2013**, *52*, 7419−7421. (e) Zhang, S.; Metin, O.; Su, D.; Sun, S. *Angew. Chem., Int. Ed.* **2013**, *52*, 3681−3684. (f) Yu, Y.; Yang, W.; Sun, X.; Zhu, W.; Li, X.-Z.; Sellmyer, D. J.; Sun, S. *Nano Lett.* **2014**, *14*, 2778−2782.

(3) (a) Farha, O. K.; Spokoyny, A. M.; Mulfort, K. L.; Hawthorne, M. F.; Mirkin, C. A.; Hupp, J. T. *J. Am. Chem. Soc.* **2007**, *129*, 12680−12681. (b) Chen, B.; Zhao, X.; Putkham, A.; Hong, K.; Lobkovsky, E. B.; Hurtado, E. J.; Fletcher, A. J.; Thomas, K. M. *J. Am. Chem. Soc.* **2008**, *130*, 6411−6423. (c) Fellay, C.; Dyson, P. J.; Laurenczy, G. *Angew. Chem., Int. Ed.* **2008**, *47*, 3966−3968. (d) Jiang, H.-L.; Singh, S. K.; Yan, J.-M.; Zhang, X.-B.; Xu, Q. *ChemSusChem* **2010**, *3*, 541−549. (e) Boddien, A.; Loges, B. r.; Gärtner, F.; Torborg, C.; Fumino, K.; Junge, H.; Ludwig, R.; Beller, M. *J. Am. Chem. Soc.* **2010**, *132*, 8924−8934. (f) Boddien, A.; Mellmann, D.; Gartner, F.; Jackstell, R.; Junge, H.; Dyson, P. J.; Laurenczy, G.; Ludwig, R.; Beller, M. *Science* **2011**, *333*, 1733−1736. (g) Bardhan, R.; Ruminski, A. M.; Brand, A.; Urban, J. J. *Energy Environ. Sci.* **2011**, *4*, 4882−4895. (h) Jeon, K.-J.; Moon, H. R.; Ruminski, A. M.; Jiang, B.; Kisielowski, C.; Bardhan, R.; Urban, J. J. *Nat. Mater.* **2011**, *10*, 286−290.

(4) (a) Yan, J.-M.; Zhang, X.-B.; Han, S.; Shioyama, H.; Xu, Q. *Angew. Chem., Int. Ed.* **2008**, *47*, 2287−2289. (b) Kim, S.-K.; Han, W.-S.; Kim, T.-J.; Kim, T.-Y.; Nam, S. W.; Mitoraj, M.; Piekos, L.; Michalak, A.; Hwang, S.-J.; Kang, S. O. *J. Am. Chem. Soc.* **2010**, *132*, 9954−9955. (c) Metin, O. n.; Mazumder, V.; Ozkar, S.; Sun, S. *J. Am. Chem. Soc.* **2010**, *132*, 1468−1469. (d) Jiang, H.-L.; Xu, Q. *Catal. Today* **2011**, *170*, 56−63. (e) Hung, T.-F.; Kuo, H.-C.; Tsai, C.-W.; Chen, H. M.; Liu, R.-S.; Weng, B.-J.; Lee, J.-F. *J. Mater. Chem.* **2011**, *21*, 11754−11759. (f) Sanyal, U.; Demirci, U. B.; Jagirdar, B. R.; Miele, P. *ChemSusChem* **2011**, *4*, 1731−1739. (g) Neiner, D.; Karkamkar, A.; Bowden, M.; Joon Choi, Y.; Luedtke, A.; Holladay, J.; Fisher, A.; Szymczak, N.; Autrey, T. *Energy Environ. Sci.* **2011**, *4*, 4187−4193. (h) Yadav, M.; Xu, Q. *Energy Environ. Sci.* **2012**, *5*, 9698−9725. (i) Huang, Z.; Autrey, T. *Energy Environ. Sci.* **2012**, *5*, 9257−9268.

(5) (a) Singh, S. K.; Xu, Q. *J. Am. Chem. Soc.* **2009**, *131*, 18032−18033. (b) Singh, S. K.; Singh, A. K.; Aranishi, K.; Xu, Q. *J. Am. Chem. Soc.* **2011**, *133*, 19638−19641. (c) He, L.; Huang, Y.; Wang, A.; Wang, X.; Chen, X.; Delgado, J. J.; Zhang, T. *Angew. Chem., Int. Ed.* **2012**, *51*, 6191−6194. (d) Singh, S. K.; Xu, Q. *Catal. Sci. Technol.* **2013**, *3*, 1889−1900. (e) He, L.; Huang, Y.; Wang, A.; Liu, Y.; Liu, X.; Chen, X.; Delgado, J. J.; Wang, X.; Zhang, T. *J. Catal.* **2013**, *298*, 1−9.

(6) (a) He, T.; Wu, H.; Wu, G.; Wang, J.; Zhou, W.; Xiong, Z.; Chen, J.; Zhang, T.; Chen, P. *Energy Environ. Sci.* **2012**, *5*, 5686−5689. (b) Wu, H.; Zhou, W.; Pinkerton, F. E.; Udovic, T. J.; Yildirim, T.; Rush, J. J. *Energy Environ. Sci.* **2012**, *5*, 7531−7535. (c) Moury, R.; Moussa, G.; Demirci, U. B.; Hannauer, J.; Bernard, S.; Petit, E.; van der Lee, A.; Miele, P. *Phys. Chem. Chem. Phys.* **2012**, *14*, 1768−1777.

(7) (a) Hannauer, J.; Akdim, O.; Demirci, U. B.; Geantet, C.; Herrmann, J.-M.; Miele, P.; Xu, Q. *Energy Environ. Sci.* **2011**, *4*, 3355−3358. (b) Zhong, D.-C.; Aranishi, K.; Singh, A. K.; Demirci, U. B.; Xu, Q. *Chem. Commun.* **2012**, *48*, 11945−11947. (c) Li, C.; Dou, Y.; Liu, J.; Chen, Y.; He, S.; Wei, M.; Evans, D. G.; Duan, X. *Chem. Commun.* **2013**, *49*, 9992−9994.

(8) (a) Cakanyıldırım, C.; Demirci, U. B.; Sener, T.; Xu, Q.; Miele, P. *Int. J. Hydrogen Energy* **2012**, *37*, 9722−9729. (b) Hannauer, J.; Demirci, U. B.; Geantet, C.; Herrmann, J.-M.; Miele, P. *Int. J. Hydrogen Energy* **2012**, *37*, 10758−10767. (c) Sener, D.; Karahan, S.; Zahmakiran, M.; Ozkar, S. *Int. J. Hydrogen Energy* **2012**, *37*, 5143−

5151. (d) Karahan, S.; Zahmakiran, M.; Ozkar, S. *Dalton Trans.* **2012**, *41*, 4912−4918.
(9) (a) Jeon, S.-i.; Park, H.-r.; Yeo, J.-g.; Yang, S.; Cho, C. H.; Han, M. H.; Kim, D. K. *Energy Environ. Sci.* **2013**, *6*, 1471−1475. (b) Zhu, Q.-L.; Tsumori, N.; Xu, Q. *Chem. Sci.* **2014**, *5*, 195−199.
(10) (a) Aranishi, K.; Singh, A. K.; Xu, Q. *ChemCatChem* **2013**, *5*, 2248−2252. (b) Singh, A. K.; Xu, Q. *ChemCatChem* **2013**, *5*, 3000−3004.
(11) (a) Scholten, J. J. F.; Pijpers, A. P.; Hustings, A. M. L. *Catal. Rev.: Sci. Eng.* **1985**, *27*, 151−206. (b) Carabineiro, S. A. C.; Machado, B. F.; Bacsa, R. R.; Serp, P.; Drazic, G.; Faria, J. L.; Figueiredo, J. L. *J. Catal.* **2010**, *273*, 191−198. (c) Long, J.; Liu, H.; Wu, S.; Liao, S.; Li, Y. *ACS Catal.* **2013**, *3*, 647−654.
(12) Boudart, M. *Chem. Rev.* **1995**, *95*, 661−666.
(13) (a) Deivaraj, T. C.; Chen, W.; Lee, J. Y. *J. Mater. Chem.* **2003**, *13*, 2555−2560. (b) Lima, F. H. B.; Salgado, J. R. C.; Gonzalez, E. R.; Ticianelli, E. A. *J. Electrochem. Soc.* **2007**, *154*, A369−A375. (c) Loukrakpam, R.; Luo, J.; He, T.; Chen, Y.; Xu, Z.; Njoki, P. N.; Wanjala, B. N.; Fang, B.; Mott, D.; Yin, J.; Klar, J.; Powell, B.; Zhong, C.-J. *J. Phys. Chem. C* **2011**, *115*, 1682−1694.
(14) Henglein, A. *J. Phys. Chem. B* **2000**, *104*, 6767−6772.
(15) Yan, J.-M.; Zhang, X.-B.; Akita, T.; Haruta, M.; Xu, Q. *J. Am. Chem. Soc.* **2010**, *132*, 5326−5327.
(16) Singh, A. K.; Xu, Q. *Int. J. Hydrogen Energy* **2014**, *39*, 9128−9134.